infrastructures

MDPI

Article

Synergistic Enhancement of Foamed Concrete Performance with Fibers and Additives Under Low-Temperature Environments and Mix Proportion Optimization

Yufeng Xian [1,2], Yaning Zhang [1,2], Zunqing Liu [1,2,*], Haiwei Xie [1,2] and Yifei Wang [1,2]

[1] School of Transportation and Logistics Engineering, Xinjiang Agricultural University, Urumqi 830052, China; 320242621@stu.xjau.edu.cn (Y.X.); 320242619@stu.xjau.edu.cn (Y.W.)
[2] Key Laboratory of Transportation and Logistics Engineering in Xinjiang, Xinjiang Agricultural University, Urumqi 830052, China
* Correspondence: liuzunqing@xjau.edu.cn

Abstract

To address the technical challenges of hydration retardation and low early strength of foamed concrete in low-temperature environments of cold regions, this study investigated the effects of low-temperature curing (cycling between −5 °C and 5 °C) on the mechanical properties and microstructure of foamed concrete. Single-factor experiments were conducted to explore the effects of triethanolamine (TEA), urea, and polypropylene fibers (PPF) on the mechanical performance of foamed concrete. A response surface methodology (RSM) was employed to establish regression models between the dosages of each component and the compressive strength (CS), thereby determining the optimal mix proportion under low-temperature curing. The experimental results indicate that increasing the urea dosage leads to an increase in the flowability of foamed concrete, and the effects of the three types of admixtures on the CS all exhibit a non-linear characteristic that first increases and then decreases. The significance of the three factors on the CS of the material follows the order: TEA > PPF > urea. The obtained optimal mix proportion is 0.052% TEA, 1.08% urea, and 0.194% PPF, yielding 3, 7, and 28 d CS of 1.088 MPa, 1.342 MPa, and 2.301 MPa, respectively. Microstructural analysis via SEM observations and XRD analysis suggest that the admixtures effectively compensate for the hydration retardation induced by low temperatures, promoting the abundant generation of needle-like ettringite (AFt) and C-S-H gels that interweave into a dense network, thereby achieving higher strength. This study provides a theoretical basis and technical support for the low-temperature construction of foamed concrete subgrades in cold regions.

Keywords: foamed concrete; low-temperature environment; admixtures; mechanical properties; response surface methodology (RSM); microstructure

Check for updates

Academic Editors: Jingbin Yang, Kang Gu, Taotao Feng and Chun-Ran Wu

Received: 26 June 2026
Revised: 3 August 2026
Accepted: 4 August 2026
Published: 6 August 2026

Copyright: © 2026 by the authors. Licensee MDPI, Basel, Switzerland. This article is an open access article distributed under the terms and conditions of the Creative Commons Attribution (CC BY) license.

1. Introduction

With the advancement of the "Belt and Road" initiative, Xinjiang has emerged as the core hub of the Silk Road Economic Belt, driving increasing demand for transportation infrastructure in alpine regions. The alpine permafrost widely distributed across this area is highly sensitive to thermal variations [1]. The construction and operation of highways inevitably impose anthropogenic thermal perturbations on the foundation, disrupting its pristine isothermal state and inducing permafrost thaw. This thermal degradation subsequently triggers engineering hazards such as differential subgrade settlement, pavement

cracking, and frost heaving, presenting severe challenges to traffic safety [2]. Mitigating these cracking risks necessitates precise prediction of restrained stress, where accounting for in situ creep is critical for accurate stress modeling [3].

A key strategy for maintaining the thermal stability of permafrost lies in constructing high-efficiency insulation layers. Organic materials, such as extruded polystyrene (XPS), have been extensively applied in permafrost engineering due to their low thermal conductivity [4]. Wang et al. [5] found that a novel double-layer polyurethane structure can serve as a "sealing cap" to block moisture migration, thereby significantly reducing thaw depth. However, these organic materials exhibit inherent deficiencies in engineering practices, such as low CS and susceptibility to degradation and aging. In contrast, foamed concrete offers several advantages in terms of mechanical performance and thermal insulation properties [6]. Generally, foamed concrete with a density class ranging from 300 to 2000 kg/m^3 possesses a thermal conductivity of 0.08–0.3 W/(m·K), offering a thermal resistance approximately 10 to 20 times that of conventional concrete [7,8]. Based on practical engineering cases, Huang et al. [9] analyzed the primary distress types and failure mechanisms in permafrost subgrades, and proposed corresponding construction techniques utilizing foamed concrete. Owing to its outstanding characteristics, load-reduction, and thermal insulation performance, foamed concrete has become a preferred solution for high-altitude highway construction in Xinjiang. It has been deployed on a large scale in key subgrade stabilization projects, including the S301 Kuixian Daban, G217 Duku Highway, and G218 Naba Expressway, validating its substantial application potential through engineering practice.

Nevertheless, during construction in the high-altitude mountainous areas of Xinjiang, the prolonged low-temperature environment severely hinders the development of early-age strength, representing a critical technical challenge that requires urgent resolution. Ning et al. [10] noted that low-temperature curing exerts a significant inhibitory effect on the microstructural evolution and mechanical property development of concrete. Taking the G218 Naba Expressway as an example, the average daily temperature during the construction period remains between −5 °C and 5 °C. In such a low-temperature environment, foamed concrete construction faces dual physical and chemical predicaments: on one hand, the hydration kinetics of cement are severely retarded, resulting in sluggish early-age strength growth; on the other hand, the volume expansion of mixing water during ice crystallization directly punctures and destroys the bubble walls. This structural damage abnormally increases pore connectivity, leading to a drastic degradation in durability [11,12]. To counteract the slow cement hydration at low temperatures, extensive research has been conducted worldwide. Huang et al. [13] found that under large diurnal temperature variations, foamed concrete with a water-cement ratio of 0.5 exhibits better environmental adaptability than that with a ratio of 0.6. Regarding chemical admixtures, Demirboğa et al. [14] found that utilizing urea as an antifreeze agent significantly improves the early-age performance and microstructural integrity of concrete at temperatures above −5 °C; however, its effectiveness is limited under more severe sub-zero conditions. Mwaluwinga et al. [15] and Wang et al. [16] reported that urea can effectively mitigate hydration heat and markedly improve the flowability, shrinkage strain, and carbonation resistance of concrete. Han et al. [17] and Ramachandran [18] revealed that TEA can accelerate tricalcium aluminate C_3A hydration and promote the transformation of AFt to monosulfate calcium sulfoaluminate (AFm), thereby shortening the setting time. However, TEA exhibits a dual effect because it can inhibit alite (C3S) hydration, the primary phase responsible for strength development, resulting in a critical dosage threshold. Therefore, determining the optimal TEA dosage that balances its effects on different mineral phases is essential. Additionally, the incorporation of PPF can exert a bridging reinforcement effect

on the pore structure of foamed concrete, but dosages exceeding the threshold tend to induce extra internal voids, thereby weakening the macro-mechanical properties [19–21].

In summary, while the antifreeze and early-strength technologies for conventional concrete have been widely documented, foamed concrete is highly sensitive and unique under low-temperature frost action due to its complex pore structures and fragile bubble walls [22]. Current literature predominantly focuses on performance modifications using a single type of admixture, whereas investigations into the multi-component combined mechanisms remain sparse. Specifically, TEA accelerates early cement hydration kinetics, urea depresses the freezing point of pore solution while maintaining hydration under sub-zero conditions, and PPF bridges microcracks and reinforces fragile cellular walls. Combining these components is expected to yield a multi-level combined effect: TEA and urea cooperatively promote early hydration and microstructural densification at low temperatures, while PPF mitigates macro/micro-crack propagation induced by thermal stress and ice crystallization pressure, thereby protecting the delicate pore skeleton. Therefore, this study targets the typical cold-region engineering scenario of a −5 °C to 5 °C temperature cycle. By incorporating a composite functional admixture system (TEA-urea-PPF), this study systematically investigates its cooperative regulation on the mechanical property evolution and microstructural hydration product development of foamed concrete, and optimizes the multi-objective mix proportions via RSM. The findings aim to provide a solid theoretical basis and technical support for the low-temperature construction of foamed concrete subgrades in cold regions.

2. Experimental Program

2.1. Materials

Ordinary Portland cement (P·O 42.5 grade, Xinjiang Fukang Tianshan Cement Co., Ltd., Urumqi, China) served as the primary binder, with its physical and mechanical properties summarized in Table 1. A commercial YS-801 cement foaming agent, supplied by Beijing Yashe Building Materials Technology Co., Ltd. (Beijing, China), was utilized to produce the pre-formed foam. Industrial-grade urea (H_2NCONH_2), purity ≥99.0%, produced by Tianjin Beilian Fine Chemicals Development Co., Ltd. (Tianjin, China), was employed as the antifreeze agent. Triethanolamine (TEA), purchased from Tianjin Zhiyuan Chemical Reagent Co., Ltd. (Tianjin, China), served as the early-strength agent, with its technical specifications listed in Table 2. A JB-I standard polycarboxylate superplasticizer, a light-yellow transparent solution, was incorporated to improve workability, and its primary technical indices are presented in Table 3. Additionally, the technical properties of the PPF used in this study are detailed in Table 4.

Table 1. Technical Indicators of Cement.

Loss on Ignition (%)	Water Consumption for Standard Consistency (%)	CS (MPa)		Flexural Strength (MPa)		Setting Time (Min)	
		3 d	28 d	3 d	28 d	Initial Setting	Final Setting
2.78	25.6	25	49.8	6.4	8.7	200	270

Table 2. Key Technical Indicators of TEA.

$N(CH_2CH_2OH)_3$(%)	Relative Density	Refractive Index	Burning Residue (%)
≥99%	1.12–1.13	1.482–1.485	≤0.1

Table 3. Key Technical Indicators of superplasticizer.

Water Reduction Rate (%)	Gas Dosage (%)	Cl^- (%)	CS Ratio (%)		
			3 d	7 d	28 d
27	3.2	0.01	162	157	149

Table 4. Key Technical Indicators of PPF.

Color	Tensile Strength (MPa)	Elastic Modulus (MPa)	Diameter (μm)	Length (mm)
Milky white	469	4236	32.7	6

2.2. Experimental Methods

2.2.1. Mix Design and Preparation

The preparation of foamed concrete specimens was conducted in strict accordance with the Test methods for foamed concrete and its products (GB/T 43487–2023 [23]). The target wet density of the foamed concrete was set at 800 kg/m^3, with a water-cement ratio of 0.45. The foaming agent featured a dilution ratio of 40, an expansion ratio of 400, and a foam density of 50 kg/m^3. Because foam dosage is the primary factor governing the wet density of fresh slurry, preliminary trial mixtures were conducted to determine the appropriate dosage required to achieve the target wet density of 800 kg/m^3. Based on these trials, the foam dosage was determined as 7% of the cement mass. To evaluate the material properties, the mixture was cast into cubic specimens with dimensions of 100 mm × 100 mm × 100 mm.

Distinct curing strategies were intentionally implemented for the single-factor experiments and the RSM optimization, primarily governed by the early-age hardenable characteristics of the matrix under sub-zero conditions. In the single-factor experimental phase, the control group (without any admixtures) failed to achieve the minimum required demolding strength under continuous sub-zero temperatures due to the severe retardation of cement hydration. Consequently, to establish a unified and feasible molding baseline across all the single-factor groups, these specimens were initially cured at ambient temperature for 12 h until demolding strength was achieved. Afterward, they were transferred to a constant temperature and humidity chamber under a cyclic temperature range of −5 °C to 5 °C until specified testing ages of 3, 7, and 28 d for CS and splitting strength (SS) tests. This curing temperature regime was established based on the average pavement temperature recorded from daily continuous monitoring conducted from March to November 2024 along the G218 Naba Expressway (the field-measured data and the simulated laboratory temperature profile are presented in Figure 1 and Figure 2, respectively). To reproduce diurnal temperature fluctuations, each temperature cycle lasted 24 h and consisted of four stages: cooling from +5 °C to −5 °C over 8 h (−1.25 °C/h), holding at −5 °C for 4 h, heating from −5 °C to +5 °C for 8 h (1.25 °C/h), and a high-temperature holding phase at +5 °C for 4 h. The specimens were not externally saturated with water during or after curing. Conversely, for the RSM optimization phase, since all the formulations contained composite early-strength and antifreeze components that imparted immediate cryo-protection, the specimens were directly placed into the −5 °C to 5 °C cyclic temperature environment immediately after casting, and cured until 3, 7, and 28 d for CS testing.

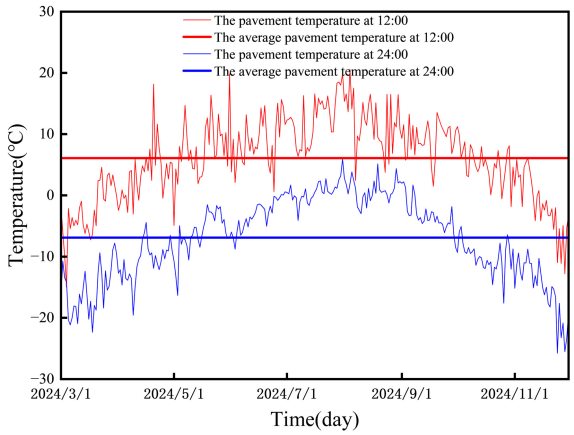


Figure 1. Road surface temperature map.

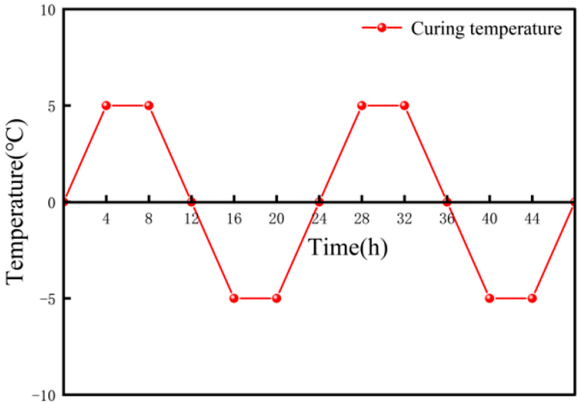


Figure 2. Curing temperature profile.

The 12 h ambient-temperature pre-curing period in the single-factor experiments provided a critical window for initial C-S-H gel nucleation and capillary skeleton formation, resulting in a substantially higher early degree of hydration compared to the RSM groups subjected to direct sub-zero curing. Consequently, the single-factor specimens systematically exhibited higher absolute macro-mechanical strength values at corresponding ages. While this methodological distinction allowed the single-factor stage to isolate individual additive trends under a feasible curing condition, it directly limits the direct quantitative comparison of absolute strength parameters between the two experimental stages. Therefore, this procedural difference constitutes a limitation of the present study.

2.2.2. Single-Factor Experiments Design

The preliminary dosage ranges were selected as follows: 0.1% to 0.4% for PPF, 0% to 5% for urea, and 0% to 0.06% for TEA. By performing CS and SS tests, the influence laws of each individual factor on the mechanical strength of the specimens were evaluated. These findings subsequently served to establish the optimal ranges and specific factor-level thresholds for the subsequent RSM analysis.

2.2.3. Response Surface Methodology Experiments Design

To further elucidate the multi-component synergistic interactions among the variables, a Box–Behnken design (BBD) was employed to construct multi-factor interaction models for the multi-objective mix optimization. The CS at specified curing ages was selected as the target response variable. For each experimental matrix point, triplicate specimens were tested and averaged to ensure a reliable statistical output. Based on the suitable dosage ranges obtained from the single-factor experiments, the dosages of urea, TEA, and PPF

were designated as the independent variables, with three distinct coding levels of −1, 0, and 1 assigned to each factor (the detailed factor levels are compiled in Table 5).

Table 5. Determination of influencing factors and levels.

Level	Factor		
	Dosage of TEA (%)	**Dosage of Urea (%)**	**Dosage of PPF (%)**
−1	0.04	0	0.1
0	0.05	1	0.2
1	0.06	2	0.3

2.3. Testing Methods

2.3.1. Physical and Mechanical Property Tests

In compliance with the Technical Specification for Application of Foamed Concrete (JGJ/T 341-2014), the flowability of the fresh slurry was evaluated. The CS and SS of the hardened foamed concrete were determined using an HYZ/YAM constant-loading rate cement testing machine. To ensure data reliability and testing precision, a constant loading rate of (2.0 ± 0.5) kN/s was strictly maintained throughout the loading process.

2.3.2. Microstructural Characterization

Scanning Electron Microscopy (SEM): Following the macro-mechanical testing, representative fractured fragments extracted from the core section of the specimens were collected as samples for microstructural analysis. These fragments were immediately immersed in anhydrous ethanol to terminate the hydration reaction. Prior to observation, the samples were oven-dried at 60 °C to a constant mass and subjected to a gold-sputtering coating treatment to impart electrical conductivity. The microstructural pore configurations and crystalline mineral morphologies were subsequently characterized using a ZEISS Sigma 300 scanning electron microscope. A total of six specimens were examined (three parallel specimens for the control group and three for the optimized compound admixture group). To ensure statistical representativeness and reproducibility, regions away from edge damage induced by mechanical fracturing were selected from the core section. For each specimen, 5–8 randomly selected fields were examined at low magnification to assess pore structure uniformity. Representative regions containing pore walls, microcracks, and hydration products were then selected for high-magnification observation.

X-ray Diffraction (XRD): The hydration-terminated samples were dried in an oven at 60 °C and then pulverized into fine powder using an agate mortar until they completely passed through a 200-mesh sieve. Phase identification was performed using a Rigaku SmartLab SE X-ray diffractometer(Rigaku Corporation, Tokyo, Japan). The scanning was executed over a 2θ angular range spanning from 5° to 80°. The measurements were conducted using Cu Kα radiation (λ = 0.15418 nm) operated at an accelerating voltage of 40 kV and a tube current of 40 mA. Data were collected in continuous scanning mode with a step size of 0.02° and a scan rate of 5°/min.

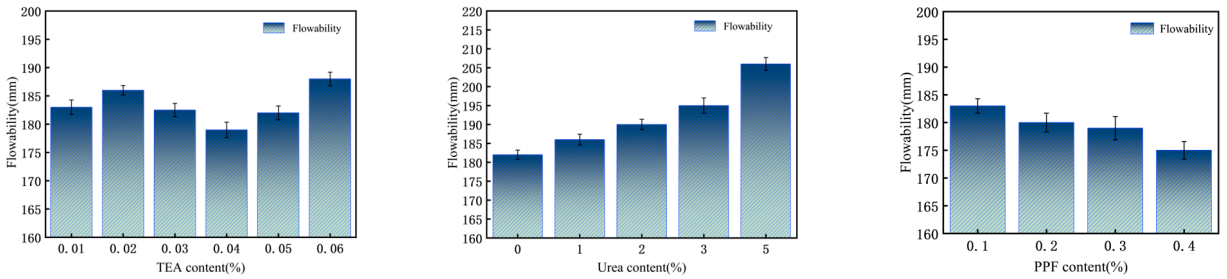
3. Results and Discussion

3.1. Single-Factor Experiments Results

3.1.1. Flowability Test

Figure 3 illustrates the effects of different admixture dosages on the flowability of the fresh foamed concrete slurry. As shown in the figure, the dosage of TEA exerts a negligible impact on the flowability, with the values remaining approximately constant at 180 mm. Conversely, urea incorporation significantly affects flowability, which increases

continuously with increasing urea dosage. In contrast, the addition of PPF leads to a progressive reduction in flowability. This retarding effect is primarily attributed to the overlapping and interlocking network of the randomly distributed PPF, which physically constrains the relative movement of the slurry, thereby elevating both the dynamic yield stress and the plastic viscosity of the fresh mixture [24].

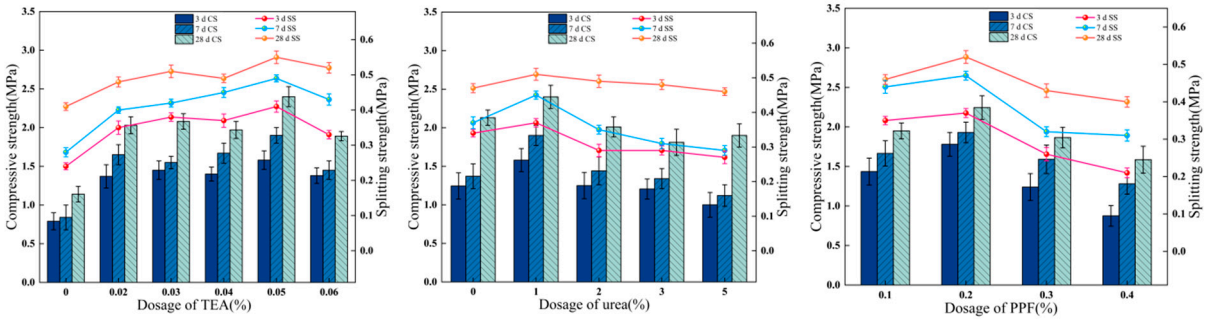


(**a**) Effect of TEA dosage on flowability (**b**) Effect of urea dosage on flowability (**c**) Effect of PPF dosage on flowability

Figure 3. Effects of various factors on flowability.

3.1.2. Mechanical Property Test

Figure 4 illustrates the influence of different admixture dosages on the CS and SS of the foamed concrete. As shown in Figure 4a, regarding the CS, the control group without TEA exhibits a 3 d CS of merely 0.79 MPa, which is significantly lower than that of the other experimental groups. This result demonstrates the limited early-age strength development of TEA-free specimens under low-temperature conditions. With the increase in TEA dosage, the CS progressively increased and reached its peak at a TEA dosage of 0.05%. Regarding the SS, its evolutionary trend is highly consistent with that of the CS, both presenting a non-linear characteristic that first increases and subsequently decreases. Notably, the SS also achieves its maximum value at the identical TEA threshold of 0.05%; this suggests that appropriate TEA accelerates C_3A hydration and rapid ettringite formation, establishing an early skeletal framework to counteract retarded hydration at low temperatures. However, when the dosage exceeds 0.05%, both the CS and SS experience a pronounced decline with further additions of TEA. This phenomenon suggests that excessive TEA addition may adversely affect strength development in foamed concrete.



(**a**) Effect of TEA dosage (**b**) Effect of urea dosage (**c**) Effect of PPF dosage

Figure 4. Effects of various factors on CS and SS.

As shown in Figure 4b, urea exerts a significant effect on the strength, characterized by an initial enhancement followed by an inhibitory action. In terms of CS, the incorporation of 1% urea increases the 3 d CS from 1.25 MPa to 1.58 MPa, indicating that 1% urea promotes early-age hydration under low temperatures. However, further increases in urea dosage resulted in a gradual reduction in strength. The SS exhibited a similar variation trend to the CS, with an initial increase followed by a subsequent decrease. Notably, the 3 d SS

of the 3% urea group was even lower than that of the control group, while the 3 d CS of the 5% urea group decreased markedly to 1.0 MPa. This reduction suggests that excessive urea may hinder hydration product formation, resulting in a looser internal structure and reduced compressive and tensile strength.

As observed from Figure 4c, PPF also exhibits a dosage-dependent effect on strength development, with an initial increase followed by a subsequent decrease. The optimal dosage of PPF was determined to be 0.2%, at which both the early-age and ultimate strengths of the foamed concrete reach their peak values, yielding a 28 d CS of 2.24 MPa and a SS of 0.52 MPa. Therefore, the incorporation of PPF effectively enhanced both the CS and SS of foamed concrete [25]. However, when the PPF dosage exceeds 0.2%, a degradation in mechanical strength is induced. This deterioration is primarily attributed to the following mechanisms: first, excessive fiber incorporation leads to fiber agglomeration that is difficult to disperse uniformly, thereby forming localized structural defects that act as stress concentration points; second, the redundant fibers can puncture or squeeze the surrounding bubbles, which abnormally increases the volume fraction of interconnected pores, consequently resulting in a sharp decline in the mechanical strength of the foamed concrete [26].

3.2. Response Surface Methodology Experiments Results

3.2.1. Compressive Strength Results and Regression Model Construction

A total of 17 experimental runs were generated utilizing the Box–Behnken design (BBD) approach. The detailed mix proportions and corresponding experimental results are compiled in Table 6 below.

Table 6. CS test results at different factor levels.

Number	TEA (%)	Urea (%)	PPF (%)	3 d CS (MPa)	7 d CS (MPa)	28 d CS (MPa)
1	0.04	0	0.2	0.66	0.94	1.67
2	0.06	0	0.2	0.76	1.17	1.9
3	0.04	2	0.2	0.76	1.14	1.76
4	0.06	2	0.2	0.82	1.11	1.92
5	0.04	1	0.1	0.75	1.18	2.06
6	0.06	1	0.1	0.77	1.12	2.13
7	0.04	1	0.3	0.72	0.93	1.77
8	0.06	1	0.3	0.92	1.15	2.15
9	0.05	0	0.1	0.67	1.12	2.01
10	0.05	2	0.1	0.81	1.27	1.99
11	0.05	0	0.3	0.84	1.15	1.88
12	0.05	2	0.3	0.81	1.11	1.91
13	0.05	1	0.2	1.08	1.32	2.25
14	0.05	1	0.2	1.12	1.37	2.34
15	0.05	1	0.2	1.05	1.33	2.28
16	0.05	1	0.2	1.07	1.31	2.32
17	0.05	1	0.2	1.11	1.35	2.24

A quadratic multiple regression analysis was performed on the experimental results of the foamed concrete. To facilitate direct application using physical dosages, all the regression models were developed using actual factor values rather than coded variables. The regression equations establishing the relationships between the admixture dosages and the CS (Y_1 for 3 d, Y_2 for 7 d, and Y_3 for 28 d CS) were constructed, as expressed in Equations (1)–(3), where X_1, X_2, and X_3 represent the dosages of TEA, urea and PPF, respectively:

$$Y_1 = -3.74775 + 161X_1 + 0.51225X_2 + 3.8075X_3 - 1X_1X_2 + 45X_1X_3 - 0.425X_2X_3 - 1642.5{X_1}^2 - 0.17175{X_2}^2 - 13.175{X_3}^2 \quad (1)$$

$$Y_2 = 2.89775 + 153.75X_1 + 0.62975X_2 - 0.0925X_3 - 6.5X_1X_2 + 70X_1X_3 - 0.475X_2X_3 - 1567.5{X_1}^2 - 0.08925{X_2}^2 - 8.425{X_3}^2 \quad (2)$$

$$Y_3 = -2.614 + 183.5X_1 + 0.6215X_2 - 2.03X_3 - 1.75X_1X_2 + 77.5X_1X_3 + 0.325X_2X_3 - 1867.5{X_1}^2 - 0.28675{X_2}^2 - 7.175{X_3}^2 \quad (3)$$

3.2.2. ANOVA and Residual Analysis

To evaluate the interactive effects of the three factors, namely the dosages of TEA (X_1), urea (X_2), and PPF (X_3), an analysis of variance (ANOVA) was performed on the regression models. The corresponding statistical parameters are summarized in Tables 7 and 8. According to the ANOVA results in Table 7, the *p*-values for all the curing-age models are lower than 0.0001, indicating an extremely significant level. These results demonstrate that the developed quadratic models can reliably describe the relationships between admixture dosages and CS. In terms of the goodness-of-fit, the *p*-values of the lack-of-fit terms for the three models are 0.7420, 0.5716, and 0.9573, respectively, all of which are substantially greater than the significance threshold of 0.05. This insignificant lack-of-fit supports that the models exhibit an excellent fit to the experimental data without omission of important terms. Regarding the significance levels of individual factors, TEA, urea, and PPF exert distinct periodic characteristics on strength development. Both TEA and PPF exhibit extreme significance across the entire curing cycle, suggesting their paramount roles in the continuous development of CS. In contrast, the influence of urea is predominantly concentrated in the early stage, with its statistical significance fading by 28 d. This phenomenon implies that urea primarily participates in the early-age cement hydration kinetics, whereas its contribution to the long-term strength evolution diminishes markedly.

Table 7. ANOVA of Regression Model for CS.

	3 d CS		7 d CS		28 d CS	
Index	**F-Value**	***p*-Value**	**F-Value**	***p*-Value**	**F-Value**	***p*-Value**
Model	70.83	<0.0001	57.41	<0.0001	69.47	<0.0001
X_1	28.75	0.0011	31.11	0.0008	76.51	<0.0001
X_2	14.51	0.0066	15.00	0.0061	4.34	0.0758
X_3	16.74	0.0046	29.41	0.0010	34.00	0.0006
X_1X_2	0.6371	0.4510	32.46	0.0007	1.06	0.3369
X_1X_3	12.90	0.0088	37.64	0.0005	20.84	0.0026
X_2X_3	11.51	0.0116	17.33	0.0042	3.66	0.0971
${X_1}^2$	180.92	<0.0001	198.68	<0.0001	127.37	<0.0001
${X_2}^2$	197.82	<0.0001	64.41	<0.0001	300.31	<0.0001
${X_3}^2$	116.41	<0.0001	57.40	0.0001	18.80	0.0034
Lack of fit	0.4317	0.7420	0.7615	0.5716	0.0975	0.9573

Table 8. Regression Model Fitting Statistics and Reliability Analysis.

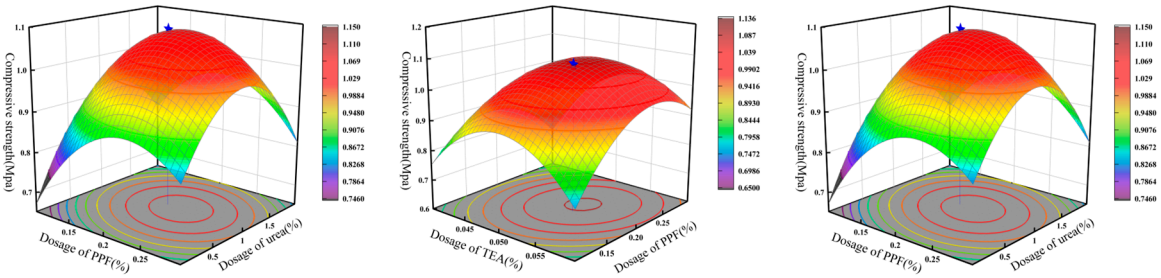
Type	**Std. Dev.**	**C.V. (%)**	**R^2**	**Adjusted R^2**	**Predicted R^2**	**Adequate Precision**
3 d CS	0.0251	2.89	0.9891	0.9752	0.9447	22.2319
7 d CS	0.0228	1.93	0.9866	0.9694	0.9090	22.8409
28 d CS	0.034	1.67	0.9889	0.9747	0.9718	23.8467

According to the analysis in Table 8, the coefficients of determination R^2 for all three curing ages exceed 0.98, and the adjusted R^2 values are all greater than 0.96. These statistical indicators demonstrate that the designated model terms are appropriate, imparting the regression models with superior accuracy and robust reliability. Furthermore, the

discrepancy between the adjusted R^2 and the predicted R^2 is far below the threshold of 0.2, which supports that the constructed models possess an excellent predictive capability for experimental outcomes.

3.2.3. Interaction Analysis via Response Surface Methodology

The individual effects of each factor and their mutual interactions on the 3 d CS are illustrated in Figure 5. As shown in Figure 5a, when the PPF dosage is fixed at the central level, the CS exhibits an initial increase followed by a subsequent decrease with the escalating dosages of both TEA and urea. Notably, the response curve of TEA is significantly steeper than that of urea. Concurrently, the *F*-value of TEA reaches 28.75, which is substantially higher than that of urea (14.51), indicating that TEA had a greater contribution and statistical significance to early-age strength development. Based on the response surfaces in Figure 5b,c, when either urea or TEA is kept constant, the CS presents a typical dome-shaped distribution as a function of the other chemical admixture and the PPF dosage. The interaction between TEA and PPF was highly significant, indicating a synergistic effect between TEA-induced acceleration of hydration kinetics and PPF-induced physical bridging during early-age strength development. In terms of sensitivity, the early-age CS shows the highest sensitivity to the TEA dosage, followed by the PPF dosage, while the urea dosage exerts the mildest influence. In summary, the hierarchy of the factors influencing the 3 d CS is determined as follows: TEA > PPF > urea. This sequence is closely related to their underlying physical and chemical mechanisms: TEA acts as a powerful catalyst that accelerates cement hydration kinetics, serving as the primary driving force for early-age strength growth [27]. Meanwhile, the randomly distributed fibers provide a stable mechanical skeleton via their physical bridging effect within the nascent hydration products.

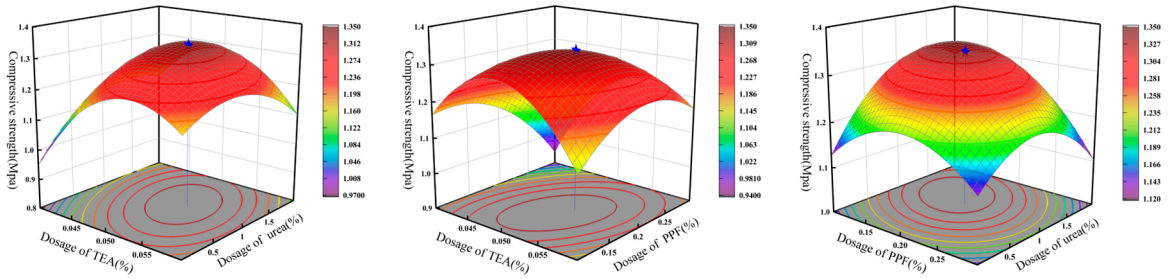


(**a**) TEA-urea Surface Plot (**b**) TEA-PPF Surface Plot (**c**) PPF-urea Surface Plot

Figure 5. Response surface plots showing the effects of various factors on 3 d CS. The star symbol indicates the optimal mix ratio calculated by the optimization software.

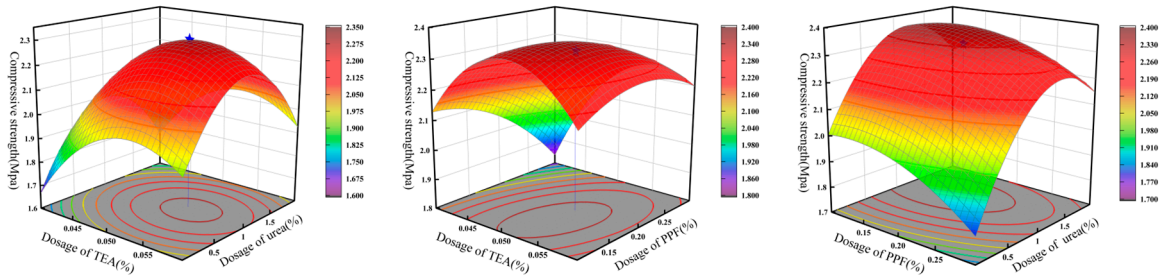
The individual effects of each factor and their interactions on the 7 d CS are illustrated in Figure 6. While the hierarchy of single factors remains consistent with the 3 d stage (TEA > PPF > urea), the interaction dynamics undergo a distinct transition. The interaction between TEA and urea plays a critical role. While their interaction is statistically insignificant at the 3 d curing age, it reaches a highly significant level ($p < 0.0001$) by 7 d. This transition reflects that with the progression of cement hydration, the synergistic chemical reactions between the alkaline environment provided by TEA and the chemical constituents of urea deliver an increasingly prominent contribution to the subsequent strength evolution.

The individual effects of each factor and their mutual interactions on the 28 d CS are illustrated in Figure 7. Although the single-factor hierarchy consistently maintains the order of TEA > PPF > urea across all the curing ages, the individual impacts exhibit distinct features at 28 d compared to earlier stages.



(**a**) TEA-urea Surface Plot (**b**) TEA-PPF Surface Plot (**c**) PPF-urea Surface Plot

Figure 6. Response surface plots showing the effects of various factors on 7 d CS. The star symbol indicates the optimal mix ratio calculated by the optimization software.



(**a**) TEA-urea Surface Plot (**b**) TEA-PPF Surface Plot (**c**) PPF-urea Surface Plot

Figure 7. Response surface plots showing the effects of various factors on 28 d CS. The star symbol indicates the optimal mix ratio calculated by the optimization software.

First, the statistical significance of TEA becomes exceptionally prominent, with its *F*-value increasing to 76.51, which far exceeds those recorded at 3 and 7 d. This phenomenon indicates that TEA not only acts as a catalyst inducing early-age cement hydration, but the nascent mechanical skeleton it establishes during the initial stage also exerts a decisive influence on the ultimate strength of the material. Conversely, the statistical significance of urea experiences a pronounced decline. While urea functions as a highly significant factor during the 3 d and 7 d stages, its *p*-value shifts to a statistically insignificant level by 28 d. This evolution directly reflects that the primary role of the antifreeze agent lies in safeguarding the early-age survival environment of the fresh slurry under low-temperature frost action, whereas its direct contribution to the 28 d ultimate strength diminishes substantially.

3.2.4. Response Surface Optimization, Prediction, and Experimental Verification

Based on the constructed quadratic multiple regression models and the interaction analysis among the variables, a multi-objective optimization for the foamed concrete mix proportions was performed using the numerical optimization function in Design-Expert 13 software. As compiled in Table 9, the optimal formulation was determined as follows: a TEA dosage of 0.052%, a urea dosage of 1.08%, and a PPF dosage of 0.194%. The optimized foamed concrete achieved a 28 d CS of approximately 2.3 MPa. According to Specifications for Design of Highway Subgrades (JTG D30—2015), the minimum required strength for subgrade filling ranges from CF0.4 to CF0.8 depending on the subgrade layer depth. The achieved strength (2.3 MPa) substantially exceeds these standard requirements, providing an extra structural safety margin and improved frost durability for cold-region subgrades.

Table 9. Optimization Results of the Response Surface Model.

Item	TEA (%)	Urea (%)	PPF (%)	3 d CS (MPa)	7 d CS (MPa)	28 d CS (MPa)
Predicted value	0.052	1.080	0.194	1.088	1.342	2.301
Measured value	0.052	1.080	0.194	1.071	1.317	2.385
Relative error/%	-	-	-	1.56	1.86	3.46

The statistical comparison in the table indicates that the relative errors between the model-predicted values and the actual experimental results are all lower than 4%. (The relative error (RE, %) was calculated using Equation (4)). This narrow discrepancy supports that the derived RSM regression equations possess exceptional precision in predicting the mechanical strength of foamed concrete cured under low-temperature environments. Consequently, the constructed models exhibit a high degree of goodness-of-fit and robust reliability under multi-objective optimization constraints, thereby providing a solid scientific foundation and technical reference for the practical engineering applications of foamed concrete in cold regions.

$$RE = |\frac{Y_m - Y_p}{Y_p}| \times 100\% \quad (4)$$

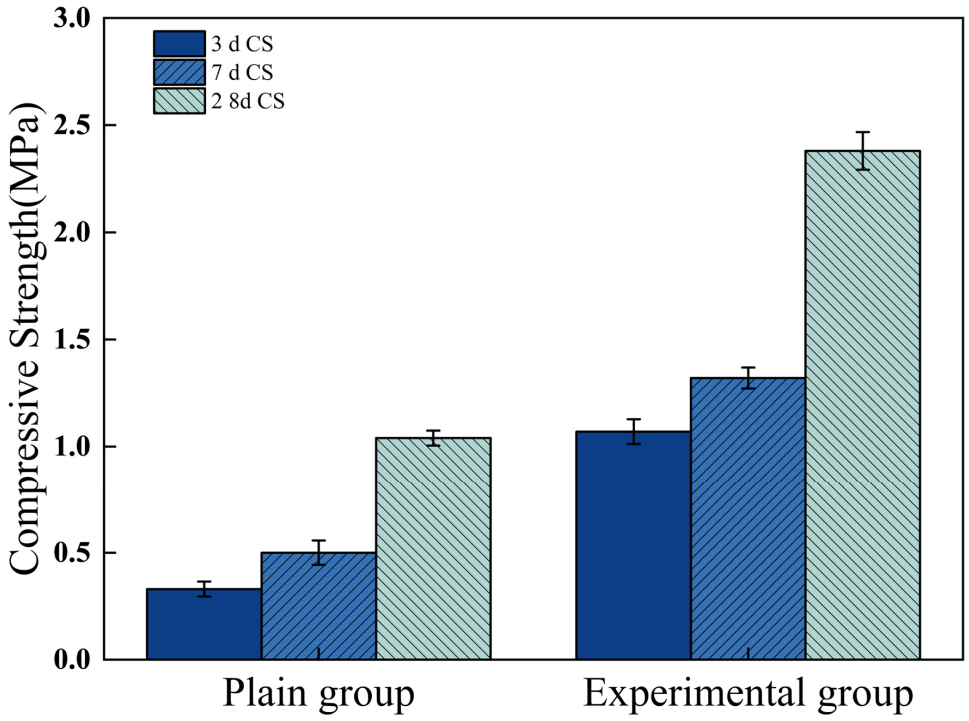
To visually verify the reinforcement performance of the compound admixtures, comparative experiments were conducted between the optimal formulation group and the blank control group (without TEA, urea, or PPF) under identical curing conditions. Each mix proportion was tested in triplicate (n = 3), and the average values of the final data were adopted. The experimental results are illustrated in Figure 8. Figure 8a visually indicates the prominent enhancement effect of the compound admixtures on mechanical strength. Under the cyclic sub-zero curing temperature range of −5 °C to 5 °C, the 3 d CS of the control group is only 0.33 MPa. In contrast, the CS of the optimized mixture increased to 1.07 MPa, approximately 3.2 times that of the control group at 3 d and comparable to the 28 d CS of the control group. This pronounced improvement supports that the incorporated chemical and physical admixtures can effectively mitigate low-temperature retardation while significantly boosting the early-age strength of the foamed concrete. As depicted in Figure 8b, the acceleration effect of the compound admixtures is particularly pronounced during the early curing stage. The mechanical strength of the blank control group develops sluggishly and is predominantly established during the later curing stages. Conversely, the admixture-modified group exhibits a distinct leftward shift in the strength growth centroid (i.e., accelerated early-stage strength kinetics), where its 3 d CS already reaches 44.6% of its 28 d ultimate strength. This behavior suggests that the combined admixtures promoted the nucleation and growth of hydration products under low-temperature conditions, thereby providing a favorable microstructural basis for subsequent strength development.

3.3. Mechanism Analysis

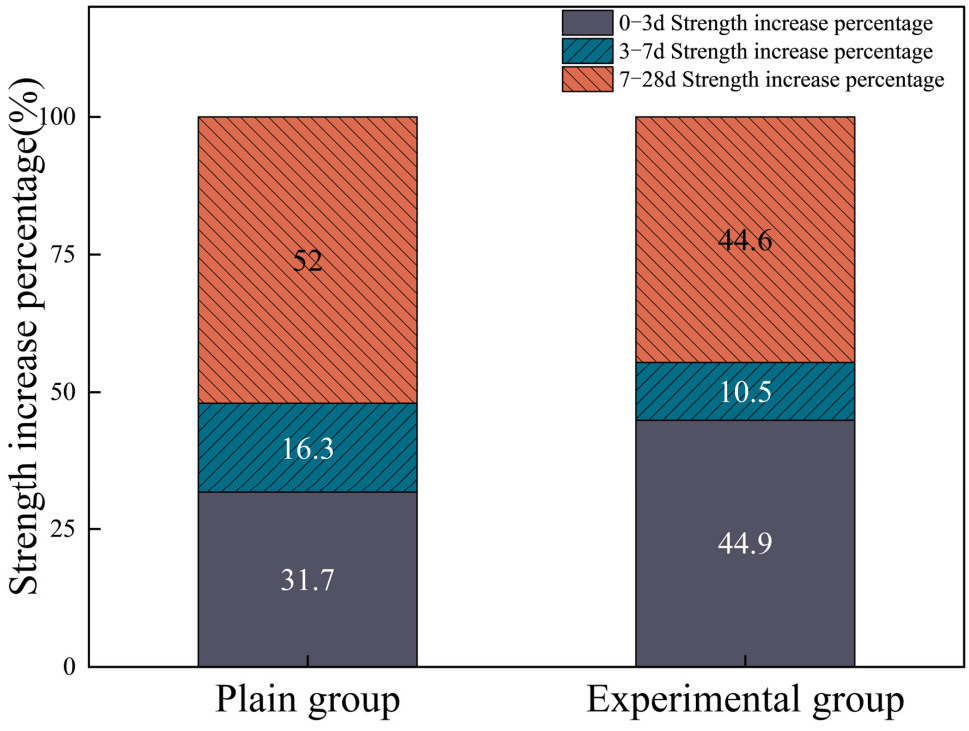
3.3.1. Microstructural Morphology Analysis

In this study, a comparative analysis was performed on the microstructural characteristics of the 7 d cured specimens containing the compound admixtures (TEA + urea + PPF) and those of the blank control group (without admixtures), as illustrated in Figure 9. It is observed that, under the synergistic effect of the compound admixtures, the pores within the foamed concrete matrix exhibit a predominantly regular spherical morphology [28], with smooth pore walls and enhanced structural continuity. The overall matrix exhibited a denser microstructure, with no obvious penetrating cracks detected. In contrast, the internal structure of the control group specimens appears relatively porous and loose, characterized by irregular pore shapes and significant inter-pore spacing. Notably, numerous

distinct cracks are observed at the boundaries and junctions of larger pores, indicating a pronounced structural brittleness and non-uniform stress distribution within the matrix.

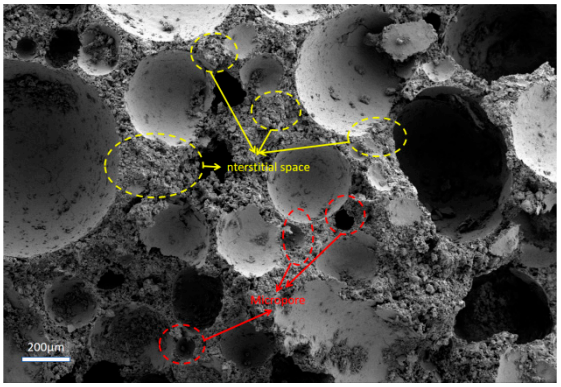


(**a**) Comparison of CS

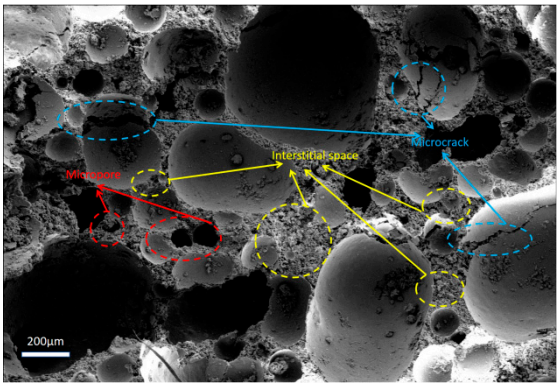


(**b**) Distribution of Strength Increase Percentages

Figure 8. Comparison of CS and strength growth between the optimal group and the blank group.



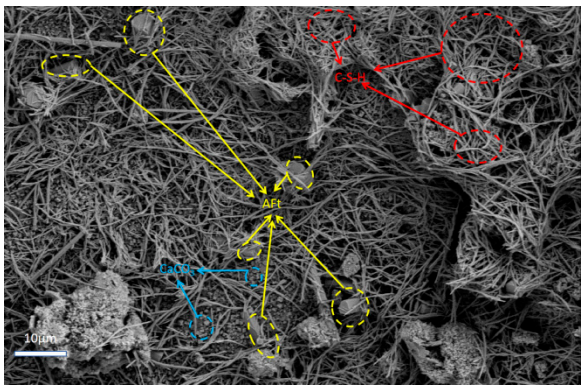
(**a**) 7 d Microstructure pore network with TEA, urea and PPF (Mag = 50×)

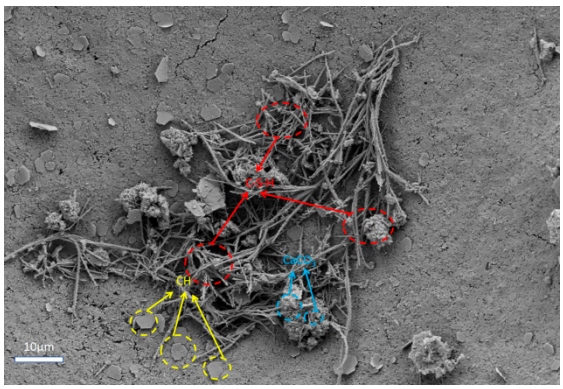


(**b**) 7 d Microstructure pore network without TEA, urea and PPF (Mag = 50×)

Figure 9. SEM images showing the macro-pore structure of foam concrete.

This microstructural enhancement is suggested to be primarily attributed to the accelerated hydration reaction of cement induced by the compound admixtures. As shown in Figure 10, the hydration process of the control group (Figure 10b) appears to be significantly inhibited under low-temperature conditions, resulting in a matrix surface with only a small number of scattered needle-like crystals and limited hydration products. In contrast, the specimens containing 0.05% TEA and 1% urea (Figure 10a) exhibit distinct microstructural characteristics. The incorporated admixtures appear to effectively compensate for the low-temperature-induced hydration retardation, facilitating the abundant growth and interweaving of needle-like AFt crystals and C-S-H gel into a dense, interconnected network [29]. This refined microstructure strengthened the pore walls, filling the structural voids, and suppressing the initiation and propagation of micro-cracks, thereby contributing to the significant improvement in the macroscopic mechanical properties of the foamed concrete.





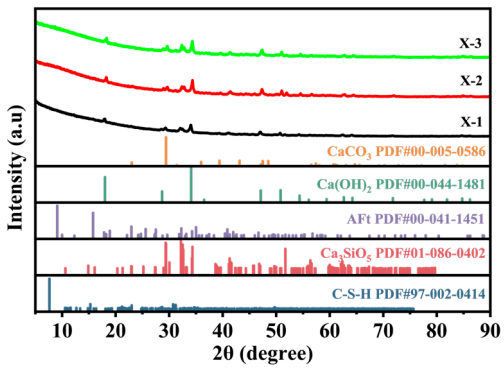
(**a**) 7 d Surface view with TEA, urea and PPF (Mag = 1000×)(**b**) 7 d Surface view without TEA, urea and PPF (Mag = 1000×)

Figure 10. SEM images of pore surface morphology.

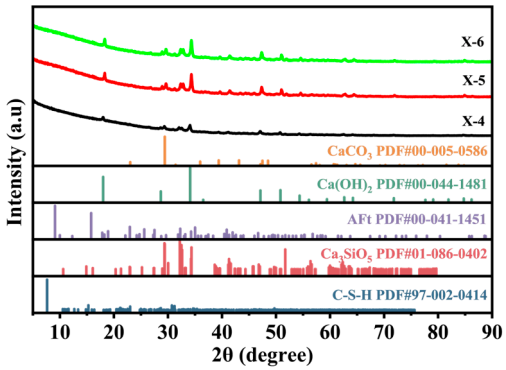
3.3.2. Hydration Products Analysis

To identify and analyze the phase composition of the hydration products in foamed concrete with varying dosages of TEA and urea, X-ray diffraction (XRD) characterization was conducted. In Figure 11a, X-1, X-2, and X-3 correspond to TEA dosages of 0, 0.05%, and 0.06%, respectively. In Figure 11b, X-4, X-5, and X-6 represent urea dosages of 0, 1%, and 3%, respectively. Comparison of the diffraction peak intensities supports that the characteristic peaks of AFt and calcium hydroxide (CH) in samples X-2 and X-3 were significantly stronger than those in the control sample X-1. This observation is consistent with the hypothesis that TEA markedly accelerates the early-stage reactions between aluminates and gypsum, as well as the overall hydration degree of silicates. Furthermore, the peak intensities for

X-2 and X-3 are remarkably similar, suggesting that a TEA dosage of 0.05% approaches the saturation threshold for its synergistic effect in this system.



(**a**) X-ray diffraction patterns of foamed concrete with different TEA dosages



(**b**) X-ray diffraction patterns of foamed concrete with different urea dosages

Figure 11. XRD patterns of foamed concrete with different additive dosages.

As suggested by the XRD patterns, the incorporation of a small amount of urea leads to a substantial increase in the diffraction peak intensities of AFt and CH, indicating that urea effectively accelerates the conversion of clinker minerals into strengthening hydration phases by optimizing the ionic environment at low temperatures. However, when the urea dosage increases to 3%, the peak intensities of the major hydration products decrease compared to the 1% dosage group. This finding implies that under low-temperature conditions, urea exerts a promotional effect on the hydration of foamed concrete at low dosages. Conversely, an excessive dosage of urea exhibits an inhibitory effect on the formation of hydration products.

4. Conclusions and Recommendations

Based on the experimental investigation and analysis, the following conclusions are drawn:

(1) Single-factor experiments indicate that urea dosage exhibits a positive correlation with the flowability of the foamed concrete, whereas PPF dosage exhibits a negative correlation. The effects of TEA, urea, and PPF on CS all follow an "increase-then-decrease" trend, with optimal dosage ranges identified as 0.04–0.06%, 0–2%, and 0.1–0.3%, respectively.

(2) RSM models demonstrate an excellent goodness-of-fit ($R^2 > 0.98$), verifying that the significance hierarchy of factors influencing the CS is TEA > PPF > urea. Based on the optimization models, the optimal mix proportions for the foamed concrete were determined as 0.052% TEA, 1.08% urea, and 0.194% PPF.

(3) SEM microstructural analysis suggests that the incorporation of TEA and urea helps optimize the pore structure of the foamed concrete, appearing to result in a more refined and uniform pore size distribution. Furthermore, these admixtures appear to work synergistically to establish a denser microstructural skeleton, which likely contributes to the observed improvements in macroscopic mechanical performance.

(4) XRD phase analysis indicates that TEA and urea exert a synergistic effect on enhancing cement hydration. They appear to accelerate the hydration kinetics of aluminates and silicates, leading to an apparent increase in key hydration products, such as AFt and CH. Specifically, the hydration-promoting effect of TEA seems to approach saturation at a dosage of 0.05%, while urea exhibits a dose-dependent effect on the formation of

hydration products, characterized by promotion at moderate dosages and potential inhibition at higher dosages.

Under low-temperature curing conditions, the developed foamed concrete attained a 28 d compressive strength of approximately 2.3 MPa. From an engineering perspective, this strength level fulfills the core functional requirements for non-load-bearing thermal insulation layers and lightweight subgrade fills in cold-region highway construction. This study established an optimized mix design strategy for foamed concrete under low-temperature conditions through single-factor experiments and RSM, and clarified the strengthening mechanisms associated with TEA, urea, and PPF. However, several limitations remain to be addressed. The laboratory simulations, while based on field-measured diurnal temperature cycles, may not fully capture the complexity of real-world service conditions; thus, more diverse and stringent hygrothermal coupling conditions should be explored. Furthermore, while this study primarily focuses on early-age kinetics and 28 d mechanical strength, the long-term durability of foamed concrete, particularly its resistance to freeze–thaw cycles, remains critical for cold-region infrastructure. In addition, given the crucial role of thermal insulation in cold and seasonal frost regions, comprehensive evaluations of thermal properties—including thermal conductivity, heat capacity, and the thermal conductivity coefficient (λ)—were not covered in this strength-focused phase. Therefore, future research will systematically integrate long-term durability evaluations and detailed thermal property measurements to further evaluate the service performance and thermo-mechanical reliability of the developed foamed concrete in severe cold environments.

Author Contributions: Conceptualization, Z.L. and Y.X.; methodology, Y.X.; software, Y.X. and Y.Z.; validation, Y.X.; formal analysis, H.X.; investigation, Y.X.; resources, Z.L. and H.X.; data curation, Y.X. and Y.Z.; writing—original draft preparation, Y.X.; writing—review and editing, Z.L.,Y.Z. and Y.W.; visualization, Y.X.; supervision, Z.L.; project administration, Z.L.; funding acquisition, Z.L. All authors have read and agreed to the published version of the manuscript.

Funding: The Science and Technology Project of Xinjiang Communications Investment Group (Grant No. KSGSGCJS-24-ZXFWHT-002) and the Postgraduate Research and Innovation Project of Xinjiang Uygur Autonomous Region (Grant No. XJ2026G138).

Data Availability Statement: The original contributions presented in this study are included in the article. Further inquiries can be directed to the corresponding author.

Conflicts of Interest: The authors declare no conflict of interest.

References

1. Baral, P.; Allen, S.; Steiner, J.F.; Gurung, T.R.; McDowell, G. Climate change impacts and adaptation to permafrost change in High Mountain Asia: A comprehensive review. *Environ. Res. Lett.* **2023**, *18*, 93005. [CrossRef]
2. Gao, F.; Xianzhang, Z.; Wenhua, Z.; Shengyong, H.U.; Junhui, Z.H. Progress and prospects of road engineering disease treatment technology in permafrost regions. *J. China Foreign Highw.* **2024**, *44*, 1–16. [CrossRef]
3. Yang, G.; Zhao, H.; Hu, Z.; Zhang, W.; Xiang, Y.; Jin, M.; Wan-Wendner, R.; Liu, J. Prediction of restrained stress for UHPC: Considering relationship between long-term and in-situ creep. *Constr. Build. Mater.* **2025**, *484*, 141722. [CrossRef]
4. Zhou, Y.; Wang, X.; Guo, C.; Hu, Y.; He, F.; Liu, D.; Jiang, D. Cooling subgrade effectiveness by L-shaped two-phase closed thermosyphons with different inclination angles and XPS insulation boards in permafrost regions. *Materials* **2022**, *15*, 8470. [CrossRef] [PubMed]
5. Wang, H.; Cao, D.; Guo, C.; Wang, F.; Zhu, W. Thermal-hydro performance research of the ice-supported frozen soil roadbed after reinforcing using polyurethane. *Energy* **2025**, *338*, 138919. [CrossRef]
6. Zhuo, Z.; Ali, A.; Zhu, C.; Mehta, Y.; Lein, W.; DeCarlo, C.; Elshaer, M.; Kennedy, D. Evaluating the potential of using foamed concrete as the insulation layer for pavements in cold regions. *Constr. Build. Mater.* **2022**, *341*, 127903. [CrossRef]
7. Fu, Y.; Wang, X.; Wang, L.; Li, Y. Foam concrete: A state-of-the-art and state-of-the-practice review. *Adv. Mater. Sci. Eng.* **2020**, *2020*, 6153602. [CrossRef]

8. Wei, S.; Yiqiang, C.; Yunsheng, Z.; Jones, M. Characterization and simulation of microstructure and thermal properties of foamed concrete. *Constr. Build. Mater.* **2013**, *47*, 1278–1291. [CrossRef]
9. Huang, J.; Cai, D.; Su, Q.; Yao, H.; Fan, R.; Pei, Y.; Zhang, Z.; Luo, J. Study on frost resistance improvement of foamed concrete used as subgrade filler. *Constr. Build. Mater.* **2025**, *468*, 140446. [CrossRef]
10. Ning, J.; Yang, Z.; Xu, X. Microscopic damage mechanism and dynamic mechanical properties of concrete materials subjected to negative-temperature curing environments. *J. Build. Eng.* **2025**, *105*, 112429. [CrossRef]
11. Liu, X.; Yao, Y.; Sheng, K.; Cheng, T.; Hong, B.; Wang, Y. Effect of Wind and Temperature on the Macroscopic Properties and Microstructure of Lightweight Cellular Concrete during Pouring. *J. Mater. Civ. Eng.* **2025**, *37*, 4024458. [CrossRef]
12. Han, F.; Wang, J.; Ji, X.; Chen, S.; Liu, J.; Wu, M.; Liu, J. Insights into the hydration kinetics and microstructural evolution of ultra-high performance cementitious composite at mid-to-low curing temperatures. *Constr. Build. Mater.* **2025**, *468*, 140403. [CrossRef]
13. Huang, W.; He, J.; Jin, Y.; Lei, D. Study on the influence of large temperature difference curing on mechanical, thermal and pore structure characteristics of foamed concrete. *Constr. Build. Mater.* **2025**, *494*, 143512. [CrossRef]
14. Demirboğa, R.; Karagöl, F.; Polat, R.; Kaygusuz, M.A. The effects of urea on strength gaining of fresh concrete under the cold weather conditions. *Constr. Build. Mater.* **2014**, *64*, 114–120. [CrossRef]
15. Mwaluwinga, S.; Ayano, T.; Sakata, K. Influence of urea in concrete. *Cem. Concr. Res.* **1997**, *27*, 733–745. [CrossRef]
16. Wang, L.; Ju, S.; Chu, H.; Liu, Z.-Y.; Yang, Z.-Q.; Wang, F.-J.; Jiang, J.-Y. Hydration process and microstructure evolution of low exothermic concrete produced with urea. *Constr. Build. Mater.* **2020**, *248*, 118640. [CrossRef]
17. Han, J.; Wang, K.; Shi, J.; Wang, Y. Mechanism of triethanolamine on Portland cement hydration process and microstructure characteristics. *Constr. Build. Mater.* **2015**, *93*, 457–462. [CrossRef]
18. Ramachandran, V.S. Hydration of cement—Role of triethanolamine. *Cem. Concr. Res.* **1976**, *6*, 623–631. [CrossRef]
19. Xu, Y.; Yao, L.; Yu, X. Effect of polypropylene fibers on mechanical and wetting properties of overall superhydrophobic foamed concrete. *Constr. Build. Mater.* **2024**, *448*, 138207. [CrossRef]
20. Wu, C.; Jierula, A.; Fu, Z.; Chen, Y.; Kuang, Y.; Xia, J. Study on the mechanism of anti sulfate freeze-thaw, dry wet cycle of polypropylene fiber foam concrete. *Constr. Build. Mater.* **2025**, *463*, 140144. [CrossRef]
21. Wu, S.; Zhang, W.; Zhang, Y.; Wang, C. Arresting properties of polypropylene fiber-reinforced foamed concrete under wet-dry cycles. *Constr. Build. Mater.* **2024**, *427*, 136233. [CrossRef]
22. Bie, Y.; Ba, S.; Chen, S. Studies on foamed concrete micropores and their effects on stress distribution and heat conduction. *J. Build. Eng.* **2024**, *87*, 109152. [CrossRef]
23. *GB/T 43487-2023*; Test Methods for Foamed Concrete and Its Products. Standards Press of China: Beijing, China, 2023.
24. Liu, J.; Guo, L.; Xi, Y.; Cheng, L.; Chen, D. Study on the rheology, mechanical properties and microstructure of polypropylene fibers in different binder systems. *J. Build. Eng.* **2024**, *90*, 109491. [CrossRef]
25. Ma, Z.; Ma, C.; Du, C.; Zhang, S.; Zhang, H.; Zhang, X.; Wang, J.; Tian, M.; Wang, Y. Research on dynamic mechanical properties of polypropylene fiber-modified rubber foamed concrete. *Constr. Build. Mater.* **2023**, *404*, 133282. [CrossRef]
26. Latifi, M.R.; Biricik, Ö.; Mardani Aghabaglou, A. Effect of the addition of polypropylene fiber on concrete properties. *J. Adhes. Sci. Technol.* **2022**, *36*, 345–369. [CrossRef]
27. Zhai, Q.; Moon, J.; Hwang, I.H.; Poon, C.-S.; Kurumisawa, K. Discovering the impact of triethanolamine (TEA): How TEA dosage transforms blast-furnace slag cement hydration. *Constr. Build. Mater.* **2025**, *491*, 142576. [CrossRef]
28. Feng, W.; Jin, Y.; Zheng, D.; Fang, Y.; Dong, Z.; Cui, H. Study of triethanolamine on regulating early strength of fly ash-based chemically foamed geopolymer. *Cem. Concr. Res.* **2022**, *162*, 107005. [CrossRef]
29. Wang, W.C.; Duong, H.T.H.; Huang, W.H.; Liu, C.-C.; Lo, I.-C. The influence of temperatures on the hydration of cement paste at the early age, and behaviour of cement paste with the addition of triethanolamine (TEA) and triisopropanolamine (TIPA). *J. Adv. Concr. Technol.* **2023**, *21*, 136–150. [CrossRef]

Disclaimer/Publisher's Note: The statements, opinions and data contained in all publications are solely those of the individual author(s) and contributor(s) and not of MDPI and/or the editor(s). MDPI and/or the editor(s) disclaim responsibility for any injury to people or property resulting from any ideas, methods, instructions or products referred to in the content.